Investigation of the Electronic Structure of Tetrakis(trifluorophosphine)nickel by Photoelectron Spectroscopy with Variable Photon Energy

John G. Brennan, Jennifer C. Green,* and Catherine M. Redfern
Inorganic Chemistry Laboratory, South Parks Road, Oxford OX1 3QR
Michael A. MacDonald
S.E.R.C. Daresbury Laboratory, Daresbury, Warrington WA4 4AD

Photoelectron spectra of $[Ni(PF_3)_4]$ have been measured using synchrotron radiation. Relative partial photoionization cross-sections and photoelectron branching ratios of the valence bands (binding energy 9—21 eV) of $[Ni(PF_3)_4]$ are reported over the photon-energy range 21—100 eV. The cross-sections of the *d* bands show both a shape resonance between 30 and 50 eV and a *p–d* resonance between 70 and 100 eV. Intensity variations are interpreted in terms of the atomic orbital contributions to the molecular orbital from which ionization is taking place. The occurrence of the *p–d* resonance for a d^{10} compound is attributed to covalent mixing of *d* character into unoccupied molecular orbitals.

The photon-energy dependence of photoionization cross-sections reveals a great deal of information on electronic structure. Synchrotron radiation allows an extensive range of photon energies to be used in photoelectron experiments, illuminating the foundations and limitations of empirical intensity rules based on He I/He II differences.[1,2] Use of an angle-resolved gas-phase photoelectron spectrometer at Daresbury[3] has afforded us the opportunity of carrying out photoelectron (p.e.) spectroscopy on gas-phase transition-metal compounds over a wide photon-energy range. Experiments on $[M(CO)_6]$ (M = Cr, Mo, or W),[4] $[M(\eta^5\text{-}C_5H_5)_2]$ (M = Fe, Ru, or Os),[5] and $[U(\eta\text{-}C_8H_8)_2]$[6] reveal significant differences in behaviour between metal and ligand cross-section behaviour. Relative partial photoionization cross-sections (r.p.p.i.c.s) of the ligand bands are mainly characterized by a rapid decline with increasing photon energy, whereas r.p.p.i.c.s of the metal bands show a slower decrease with photon energy and a wealth of features.

Common among these features is observation of a *p–d* resonance in a *d*-ionization band. Such features are helpful in assigning *d* bands[4] or in indicating covalency.[5,6] A *p–d* resonance occurs when the photon energy promotes excitation of an inner *p* electron, of the same principal quantum number as the valence *d* electron ionized, to an empty *d* level, the resonance being favoured by the angular-momentum selection rule. Subsequent to excitation, a super Coster–Kronig (s.C.K.) transition may occur, whereby an electron falls back into the *p* hole and a valence *d* electron is ionized.[7] The advent of another favourable channel for ionization may lead to a substantial increase in the *d* photoionization cross-section at such photon energies. For atoms a hole in the *d* shell of a transition metal is taken to be a necessary condition for observation of a *p–d* resonance.[8]

The parallel occurrence and stoicheiometry of transition-metal trifluorophosphine complexes with metal carbonyls suggest that the nature of the M–PF_3 interaction is similar to the M–CO interaction.[9,10] Cross-section features such as resonance phenomena are a potential source of electronic structure information and may give further insight into M–PF_3 bonding.

The compound $[Ni(PF_3)_4]$ is the simplest and most volatile of the metal trifluorophosphine complexes and hence was the most obvious choice for this study. It is formally d^{10} and so may be thought to lack the incomplete *d* shell proposed as a necessary condition for such a resonant enhancement of the *d* cross-section. Trifluorophosphine has a σ lone pair which is presumed to be donated to nickel in complex formation. Ionization from the four resulting molecular orbitals (m.o.s) of a_1 and $1t_2$ symmetry is observed as two distinct bands in the p.e. spectrum[11–13] (see Figure 1). From symmetry considerations a *d* contribution may be expected to the $1t_2$ orbitals but not to the a_1 where the metal contribution must be *s* in character. In measuring the cross-sections we sought evidence of such a difference.

We present r.p.p.i.c.s and branching ratios (b.r.s) for the valence ionizations of $[Ni(PF_3)_4]$.

Experimental

A full account of our experimental method has been given[4] and the apparatus and its performance is described elsewhere,[3] therefore only a brief account of experimental procedures is given here.

Synchrotron radiation from the 2-GeV electron storage ring at S.E.R.C. Daresbury Laboratory was monochromated using a toroidal grating monochromator (t.g.m.) and was used to photoionize gaseous samples in a cylindrical ionization chamber. The t.g.m. was employed with fixed slit widths of 2 mm. Total instrumental resolution was limited by the electron pass energy and was in the range 150—600 meV. The photoelectrons were energy analysed with a three-element zoom lens in conjunction with a hemispherical electron-energy analyser which was positioned at the 'magic angle' in order to eliminate the influence of the photoelectron asymmetry parameter, β, on signal intensity. This angle is dependent on the polarization of the radiation and varies with photon energy. The polarization varied from 67 to 88% and the 'magic angle' for each compound and inert-gas spectrum was adjusted accordingly. The 'magic angle' used varied from 120.1 to 123.8°. Multiple-scan p.e. spectra were collected at each photon energy required. The decay of the storage-ring beam current was corrected for by linking the scan rate with the output from a photodiode positioned to intersect the photon beam after it had passed through the gas cell. The sensitivity of the photodiode to different radiation energies was determined by measuring the np^{-1} p.e. spectra of Ne, Ar, and Xe. These were also used to characterize and correct for a fall off in analyser collection

Non-S.I. unit employed: eV ≈ 1.60 × 10^{-19} J.

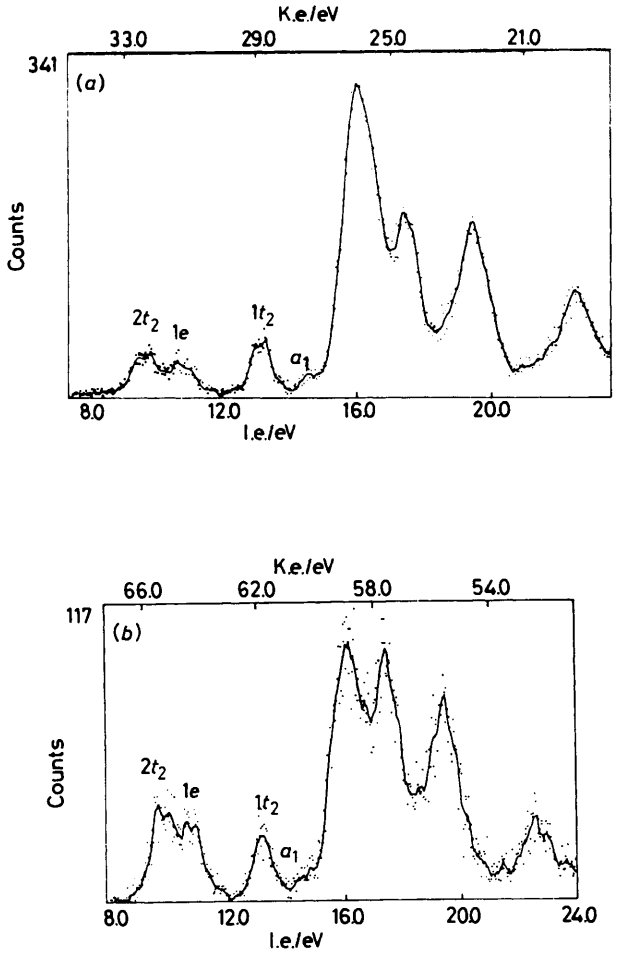

Figure 1. Photoelectron spectra of $[Ni(PF_3)_4]$, at $h\nu$ = 42 (*a*) and 75 eV (*b*); k.e. = kinetic energy, i.e. = ionization energy

Table 1. Assignment of the p.e. spectrum of $[Ni(PF_3)_4]$ [13]

Label	I.e./eV	Assignment	PF_3 parent orbital
A	9.69	$2t_2$ (Ni 3*d*)	
B	10.74	1*e* (Ni 3*d*)	
C	13.17	$1t_2$ (M–P)	$8a_1$
D	14.65	a_1 (M–P)	$8a_1$
E_1	15.97	F lone pairs	$6e$, $1a_2$
E_2	17.48	F lone pairs	$5e$
E_3	19.42	P–F bond	$4e$, $7a_1$
F	22.4	P–F bond	$6a_1$

efficiency at kinetic energies ≤15 eV. Photoionization cross-sections for the rare gases were taken from the literature.[14,15]

Trifluorophosphine PF_3 was prepared from ZnF_2 and PCl_3 using the Williams method [16] modified by sealing the reactants together in a stainless-steel reaction bottle for 24 h, rather than adding the PCl_3 continuously. The compound $[Ni(PF_3)_4]$ was prepared by metal-vapour synthesis,[17] and repeatedly purified by trap-to-trap distillation. The $[Ni(PF_3)_4]$ was sufficiently volatile that an ampoule containing it could be attached outside the spectrometer and the compound sublimed at ambient temperatures into the gas cell *via* the same line as the inert gases. A liquid-nitrogen-cooled cold finger was fitted to the spectrometer to prevent diffusion of compound into the pumps. Sample-pressure fluctuations were corrected for by collecting a 'standard' calibration spectrum before and after each data spectrum. The integrated intensities of the bands in these spectra were then used as a relative measure of the sample density in the ionization region.

Table 2. R.p.p.i.c.s and b.r.s for the nickel 3*d* localized 1*e* and $2t_2$ ionizations

	$2t_2$		1*e*	
$h\nu$ (eV)	r.p.p.i.c.	b.r.	r.p.p.i.c.	b.r.
21.0	90.9 ± 3.7	0.008 ± 0.001	57.0 ± 2.7	0.006 ± 0.001
24.0	92.3 ± 3.2	0.011 ± 0.001	53.5 ± 2.7	0.006 ± 0.001
27.0	63.4 ± 2.1	0.027 ± 0.001	39.5 ± 1.6	0.017 ± 0.001
30.0	47.2 ± 1.5	0.038 ± 0.001	36.4 ± 1.4	0.029 ± 0.001
33.0	35.5 ± 1.2	0.037 ± 0.001	26.3 ± 1.1	0.027 ± 0.001
36.0	30.2 ± 1.1	0.037 ± 0.001	27.9 ± 1.0	0.035 ± 0.001
39.0	31.11 ± 0.96	0.042 ± 0.001	26.5 ± 0.9	0.036 ± 0.001
42.0	28.44 ± 0.85	0.044 ± 0.001	21.4 ± 0.7	0.033 ± 0.001
45.0	32.06 ± 0.77	0.054 ± 0.001	20.7 ± 0.6	0.035 ± 0.001
50.0	28.60 ± 1.17	0.051 ± 0.001	16.2 ± 0.9	0.029 ± 0.001
60.0	21.1 ± 0.9	0.063 ± 0.003	12.5 ± 0.7	0.036 ± 0.002
65.0	28.8 ± 0.9	0.071 ± 0.002	17.7 ± 0.7	0.042 ± 0.002
70.0	21.4 ± 0.8	0.058 ± 0.002	17.5 ± 0.7	0.046 ± 0.002
72.5	30.87 ± 0.93	0.067 ± 0.002	23.3 ± 0.8	0.049 ± 0.002
75.0	40.12 ± 1.20	0.088 ± 0.003	33.6 ± 1.1	0.068 ± 0.002
77.5	23.9 ± 1.1	0.078 ± 0.004	19.1 ± 1.0	0.060 ± 0.003
80.0	25.9 ± 1.0	0.072 ± 0.003	21.4 ± 0.9	0.057 ± 0.003
82.5	24.4 ± 1.2	0.073 ± 0.004	17.5 ± 1.0	0.052 ± 0.003
85.0	22.3 ± 0.9	0.070 ± 0.003	19.8 ± 0.8	0.062 ± 0.003
87.5	19.5 ± 0.8	0.071 ± 0.003	16.1 ± 0.7	0.058 ± 0.003
90.0	22.4 ± 0.8	0.069 ± 0.003	21.1 ± 0.8	0.065 ± 0.003
100.0	18.4 ± 0.8	0.066 ± 0.003	15.1 ± 0.7	0.057 ± 0.003

Data Analysis

As the p.e. spectrum of $[Ni(PF_3)_4]$ contains many overlapping bands, individual r.p.p.i.c.s could not be obtained by integration. The bands were deconvoluted by fitting with symmetric Gaussian curves, the best fit being determined by a least-squares refinement. Band labels are defined in Table 1 and Figure 3. Bands C—E were fitted without applying any restraints, but to obtain reasonable fits to bands A and B their widths were constrained to be equal.

The b.r. data are independent of both the sensitivity of the photodiode to photon energy and the long-term variation in sample pressure, and are only corrected by kinetic energy calibration. For the points on the r.p.p.i.c plots, where pressure variations and photodiode calibration factors also contribute to the possible errors, relative values of points within 5 eV of each other are probably accurate to within 5%, whereas data separated by >20 eV contain a relative uncertainty of 10%. All r.p.p.i.c. features commented upon and discussed below were clearly visible in the b.r. plots.

At photon energies of 24 and 27 eV the background at the high-ionization-energy end of the spectrum was difficult to determine accurately. Consequently the width of E_3 was over exaggerated so the absolute values of the r.p.p.i.c and b.r. for bands E_1—E_3 at these energies are subject to large errors. This only affects the relative areas of the bands in region E at these energies and does not influence the r.p.p.i.c. or b.r. behaviour of bands A—D. Figure 1 shows p.e. spectra of $[Ni(PF_3)_4]$ obtained with synchrotron radiation at photon energies of 42 and 75 eV. R.p.p.i.c.s and b.r.s for the nickel 3*d* ($2t_2$ and 1*e*) and M–P ($1t_2$ and a_1) based ionizations are shown in Figures 4 and 6 respectively. These values are collected in Tables 2 and 3. Errors quoted in the Tables originate from statistical uncertainties associated with band-area measurements. The r.p.p.i.c.s and b.r.s of bands E_1—E_3 are shown in Figures 7 and 8.

Table 3. R.p.p.i.c.s and b.r.s for the nickel–phosphorus $1t_2$ and a_1 ionizations

	$1t_2$		a_1	
hν (eV)	r.p.p.i.c.	b.r.	r.p.p.i.c.	b.r.
21.0	245.7 ± 6.1	0.028 ± 0.001	110 ± 5	0.011 ± 0.001
24.0	159.8 ± 5.1	0.019 ± 0.001	59.6 ± 3.4	0.007 ± 0.001
27.0	53.7 ± 1.9	0.023 ± 0.001	10.7 ± 0.9	0.005 ± 0.001
30.0	42.1 ± 1.4	0.034 ± 0.001	5.76 ± 0.53	0.005 ± 0.001
33.0	34.7 ± 1.3	0.036 ± 0.001	9.54 ± 0.65	0.010 ± 0.001
36.0	30.6 ± 1.1	0.038 ± 0.001	7.70 ± 0.52	0.010 ± 0.001
39.0	31.53 ± 0.98	0.042 ± 0.001	5.36 ± 0.40	0.007 ± 0.001
42.0	31.56 ± 0.88	0.049 ± 0.001	4.00 ± 0.32	0.006 ± 0.001
45.0	29.01 ± 0.73	0.049 ± 0.001	2.24 ± 0.20	0.004 ± 0.001
50.0	29.14 ± 1.05	0.052 ± 0.001	3.85 ± 0.29	0.007 ± 0.001
60.0	13.9 ± 0.7	0.045 ± 0.002	3.30 ± 0.32	0.011 ± 0.001
65.0	14.8 ± 0.6	0.040 ± 0.002	3.90 ± 0.32	0.010 ± 0.001
70.0	15.7 ± 0.6	0.046 ± 0.002	5.32 ± 0.36	0.016 ± 0.001
72.5	18.61 ± 0.69	0.044 ± 0.002	3.41 ± 0.30	0.008 ± 0.001
75.0	22.35 ± 0.85	0.053 ± 0.002	3.58 ± 0.34	0.009 ± 0.001
77.5	14.4 ± 0.8	0.051 ± 0.003	1.3 ± 0.2	0.005 ± 0.001
80.0	14.0 ± 0.6	0.047 ± 0.003	2.9 ± 0.3	0.014 ± 0.001
82.5	12.7 ± 0.8	0.045 ± 0.003	3.9 ± 0.4	0.014 ± 0.002
85.0	11.1 ± 0.6	0.041 ± 0.002	1.9 ± 0.2	0.007 ± 0.001
87.5	10.8 ± 0.5	0.046 ± 0.002	3.2 ± 0.3	0.014 ± 0.001
90.0	11.1 ± 0.5	0.041 ± 0.002	2.0 ± 0.2	0.007 ± 0.001
100.0	8.8 ± 0.5	0.038 ± 0.002	2.5 ± 0.3	0.011 ± 0.001

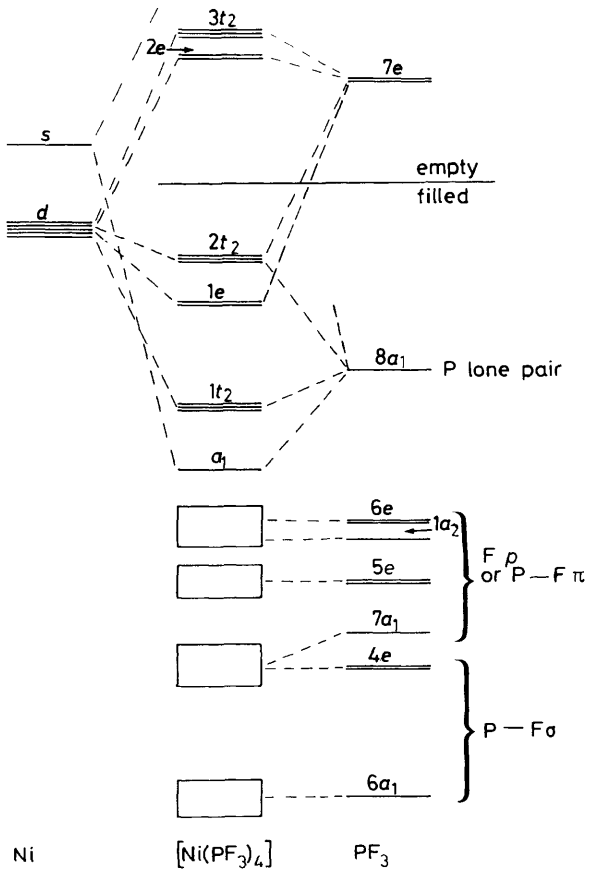

Figure 2. A schematic m.o. diagram for $[Ni(PF_3)_4]$. The Ni 4*s* and 3*d* orbitals are represented on the left; the m.o.s in the centre are for $[Ni(PF_3)_4]$ and are labelled according to the T_d point group for the upper levels; on the right are the m.o.s of PF_3 labelled according to the C_{3v} point group and according to their principal bonding type. Also indicated on the right is the level up to which the ligand and complex orbitals are filled

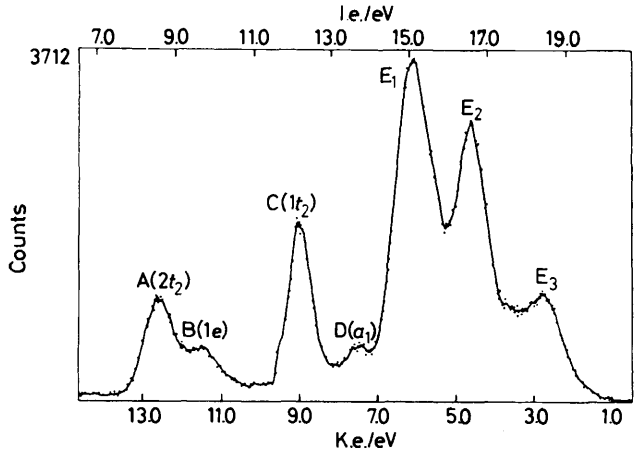

Figure 3. He I photoelectron spectrum of $[Ni(PF_3)_4]$

Results and Discussion

Bonding and Interpretation of the P.E. Spectrum.—A schematic m.o. diagram for $[Ni(PF_3)_4]$ is shown in Figure 2; the molecular levels are labelled according to the T_d symmetry of the NiP_4 core, whereas the PF_3 orbitals are labelled in the C_{3v} symmetry of the ligand. Metal–ligand σ bonding is generated primarily through interaction of the Ni 3*d* orbitals with the t_2 combination of PF_3 lone pairs and the Ni 4*s* orbitals with the a_1 combination of PF_3 lone pairs. Consequently the Ni *d* orbitals split into a triply degenerate set of nickel localized orbitals of high energy ($2t_2$) and a doubly degenerate set of lower energy ($1e$). Both these sets of orbitals are filled. The role of PF_3 as a π acceptor has been widely discussed and the evidence from both theoretical and experimental studies[18–29] indicates that there is a π interaction between PF_3 and the metal. Both the phosphorus *d* orbitals and the P–F σ* orbitals have been suggested as being the acceptor orbitals involved in the metal-to-ligand back donation. Both the *e* and the t_2 orbitals of $[Ni(PF_3)_4]$ are of the correct symmetry to back donate to the PF_3 ligands. Consequently, in tetrahedral symmetry, the *d* orbitals cannot be separated into a σ and a π set.

Figure 3 shows a labelled He I p.e. spectrum of $[Ni(PF_3)_4]$. Although there was initial conflict[11,12] over the precise assignment, widely accepted assignments of the p.e. spectrum of $[Ni(PF_3)_4]$ have now been achieved.[13] The two low-ionization-energy (i.e.) bands A and B are attributed to ionization from the $2t_2$ (A) and $1e$ (B) nickel-based 3*d* orbitals which are fully occupied in the neutral molecule. In T_d symmetry the highest occupied molecular orbitals (h.o.m.o.s) of the four PF_3 molecules combine to give orbitals of t_2 and a_1 symmetry which become Ni–P σ bonding in the complex. Band C is assigned to ionization from the $1t_2$ (M–P) orbitals and band D to ionization from the a_1 orbital. The remaining bands, E_1—E_3, are assigned to ionization from essentially PF_3 localized orbitals; E_1 and E_2 arise from ionization of F p_π orbitals, $6e$ and $1a_2$ in the case of E_1 and $5e$ in the case of E_2. The E_3 band comes from ionization of the P–F σ-bonding electrons, orbitals $7a_1$ and $4e$ in the free ligand. Band F correlates with the $6a_1$ ionization of PF_3; again P–F σ bonding, but here involving the phosphorus 3*s* orbital.[30] These assignments are summarized in Table 1.

The metal-localized $2t_2$ *and* $1e$ *bands.* The r.p.p.i.c.s and b.r.s of these bands are shown in Figure 4 and collected in Table 2. From Figure 4(*c*) it can be seen that the relative intensities of these two nickel 3*d*-based ionizations are generally in the 3:2 ratio expected on the basis of degeneracies. Deviations from this ratio occur in two photon-energy regions; 30—50 and 70—100 eV. In these regions the $1e^{-1}$ band gains in intensity with respect

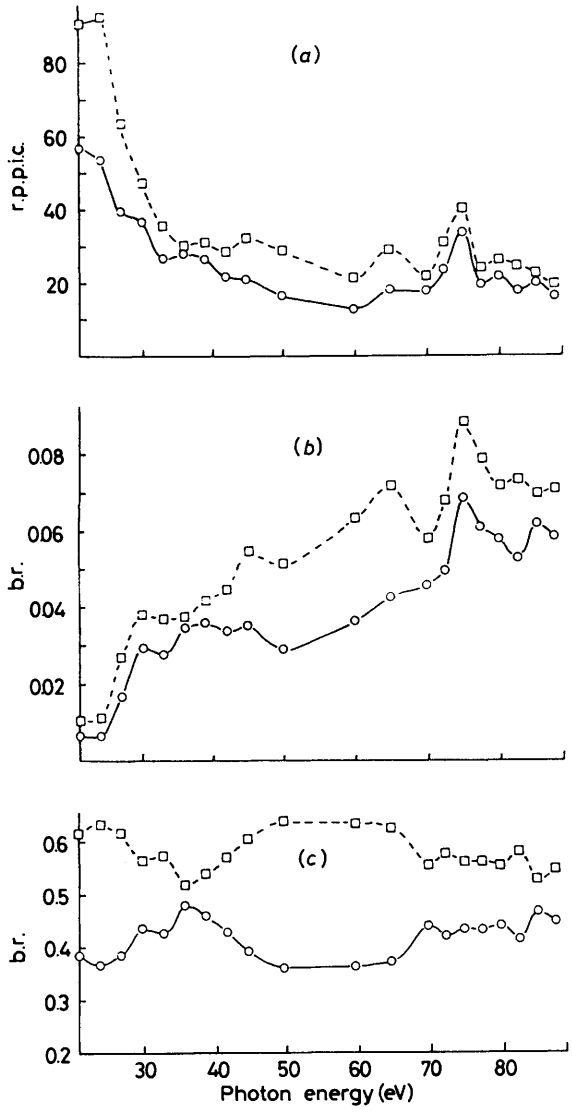

Figure 4. R.p.p.i.c.s and b.r.s for $2t_2$ (□) and $1e$ (○) orbitals: (*a*) r.p.p.i.c.s, (*b*) b.r. for $2t_2$ and $1e$ relative to whole spectrum, and (*c*) $2t_2/1e$ b.r.

to the $2t_2^{-1}$ band. As can be seen from Figure 4(*a*) and (*b*) there are two resonance features in the r.p.p.i.c.s and b.r.s of the $2t_2$ and $1e$ bands. The first is in the $h\nu$ = 30—50 eV region and is assigned to a molecular shape resonance.[31] Figure 4(*c*) shows the $1e/2t_2$ b.r. and from this it can be seen that the shape resonance is stronger for the *e* than for the t_2 orbitals. Both bands show a second maximum in their r.p.p.i.c.s at a photon energy of 75 eV. This occurs at a photon energy close to the 3*p* binding energy ($3p_{\frac{1}{2}}$ 75 eV, $3p_{\frac{3}{2}}$ 73 eV) of free nickel atoms[32] and so is assigned to the giant resonance due to $3p \longrightarrow 3d$ resonant enhancement of photoemission.

As noted in the Introduction it is a common assumption that to observe resonant enhancement of photoemission from atoms the orbital that the electron is being excited to must not be filled, so to observe $3p \longrightarrow 3d$ giant resonances the 3*d* orbitals must not be full. This is not necessarily true for molecules. The compound $[Ni(PF_3)_4]$ is formally a nickel(0) complex with a d^{10} configuration and the $2t_2$ and $1e$ orbitals, which are predominantly Ni 3*d* in character, are filled. Extended-Hückel molecular orbital (EHMO) calculations[17b] have shown that the lowest unoccupied molecular orbitals (l.u.m.o.s) and next l.u.m.o.s, $2e$, $3t_2$ respectively, though predominantly P–F localized, have a significant contribution from Ni 3*d* orbitals. Surface plots of these orbitals are shown in Figure 5 with the metal-localized $1e$ and $2t_2$ orbitals also shown for comparison. Thus, the covalent bonding in the complex makes excitation to m.o.s with Ni 3*d* character possible even for a d^{10} configuration. The $p \longrightarrow d$ resonance must arise from excitation to these antibonding orbitals, followed by s.C.K. decay. The relevant absorption and decay processes are given below.

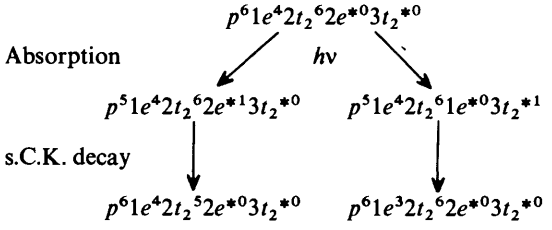

The $3p \longrightarrow$ '3*d*' absorption followed by s.C.K. decay processes shown above lead to final states identical to those obtained by direct photoionization of the metal orbitals.

As found for the shape resonance, the giant resonance is stronger in the $1e$ than the $2t_2$ band. The $2t_2$ orbitals are of the correct symmetry to have both σ and π interactions with the four PF_3 ligands, whereas the $1e$ orbitals can only undergo π interactions. Thus the $1e$ orbitals would be expected to have a higher 3*d* character than the $2t_2$ orbitals leading to the stronger resonances for this band.

The metal–phosphorus $1t_2$ *and* a_1 *orbitals.* The r.p.p.i.c.s and b.r.s for these bands are shown in Figure 6 and are collected in Table 3. The two bands differ in their behaviour over the region between 70 and 100 eV, the metal *p–d* resonance region. This is seen most clearly in the b.r.s shown in Figure 6(*b*). Figure 6(*c*) shows that the $1t_2$ orbitals gain in intensity relative to the a_1 orbitals. As the $1t_2$ orbitals can have nickel 3*d* character, they are expected to mimic the metal behaviour more closely than the a_1 orbital, which cannot mix with the Ni 3*d* orbitals. The a_1 ionization has a very low intensity and the errors in band-area measurement are large especially at the higher photon energies where counts are low. It is unlikely that the variation in r.p.p.i.c. of the a_1 band over the resonance region is statistically significant. The $1t_2$:a_1 intensity ratio varies widely over the photon-energy range studied and happens to be close to the statistical ratio of 3:1 at the He I photon energy. At the He II photon energy the $1t_2$ band has gained in intensity relative to the a_1 band as is expected from the higher Ni 3*d* character of the former.

Phosphorus 3*p* orbitals will show a Cooper minimum in their cross-sections and this is predicted to occur at a kinetic energy of 18 ± 5 eV for atomic phosphorus.[33] For the Ni–P $1t_2$- and a_1-based ionizations in $[Ni(PF_3)_4]$ (i.e.s 13.17 and 14.65 eV) this would correspond to photon energies of 31 ± 5 and 32 ± 5 eV respectively. The initial steep fall of the r.p.p.i.c. of the $1t_2$ and a_1 Ni–P σ orbitals may be due to the occurrence of the phosphorus Cooper minimum. The r.p.p.i.c.s for the a_1 orbital [Figure 6(*a*)] shows a minimum at a photon energy of 30 eV which can be assigned to the Cooper minimum of this P 3*p*-based orbital. From Figure 6(*c*) it can be seen that over the resonance regions the a_1 orbital decreases in intensity relative to the $1t_2$ orbitals. The r.p.p.i.c. behaviour of the P 3*p*-based $1t_2$ orbitals has been modified by an admixture of Ni 3*d* orbitals. The initial fall off in r.p.p.i.c.s for the $1t_2$ orbitals is less steep than that of a_1 and there is no minimum at 30 eV.

The trifluorophosphine-localized orbitals. Initially these bands, E_1—E_3, show a rapid fall in cross-section as the photon energy is increased (see Figure 7). This is the

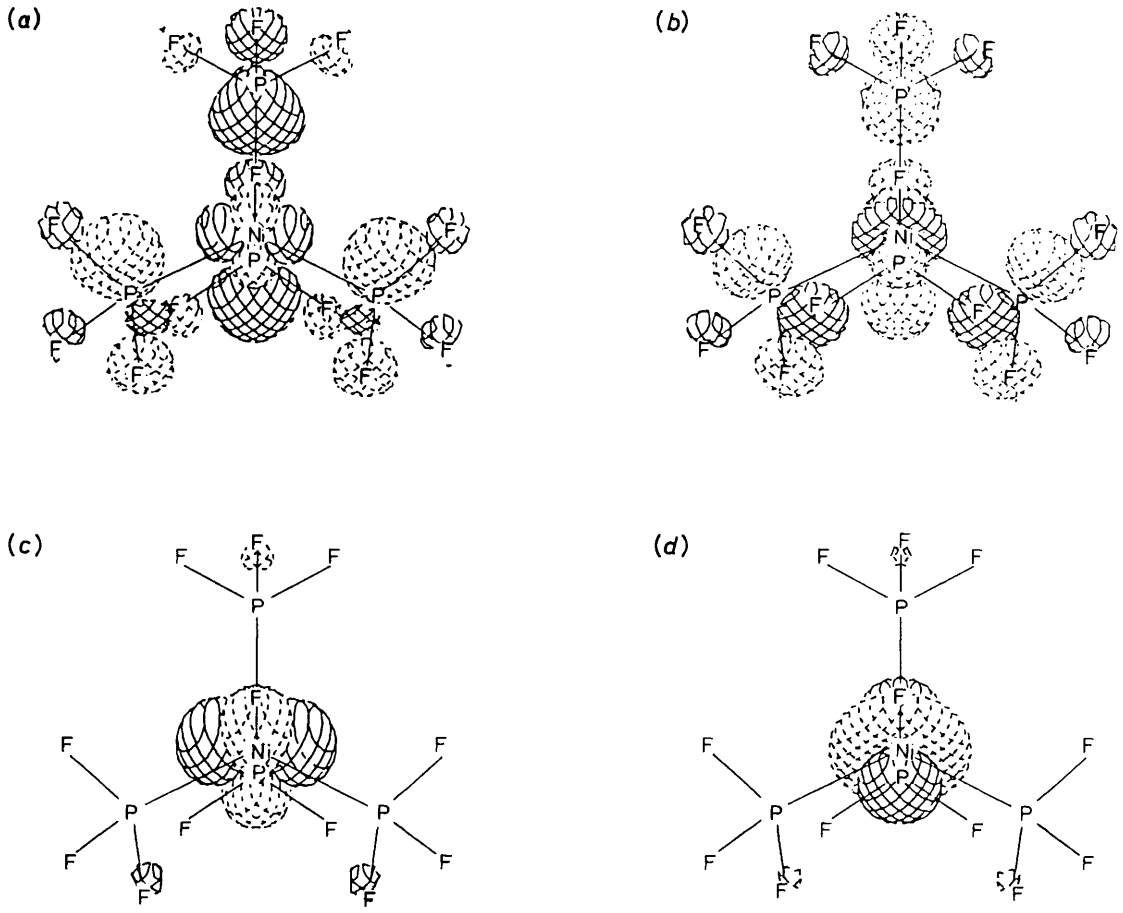

Figure 5. Surface plots for the m.o.s of $[Ni(PF_3)_4]$: (*a*) $3t_2$, (*b*) $2e$ (l.u.m.o.), (*c*) $2t_2$ (h.o.m.o.), and (*d*) $1e$

behaviour that is predicted for predominantly F $2p$ and P $3p$ localized orbitals on the basis of the Gelius model. Calculations on atomic P and F predict this rapid fall off in cross-section[33] and it has been observed for F-based orbitals in many fluorocarbons.[3,34–37]

As noted above high background in the region of band E at photon energies <30 eV precludes accurate estimates of branching ratios. Consequently these are only given at energies 30 eV and above (Figure 8) and comparison of the behaviour of bands E_1, E_2, and E_3 is based on the data between 30 and 100 eV.

Inspection of Figure 7(*a*) shows that the fall off in intensity above 30 eV is less steep for the E_1 band than for E_2 or E_3, which behave in a very similar fashion between photon energies 30 and 70 eV. A decrease in the intensity of E_2 with respect to E_1 with increase in photon energy is also evident from the He I and He II spectra of PF_3.[30,38] A reasonable explanation for this intensity variation is that the orbitals giving rise to bands E_2 and E_3 have significant P $3p$ character, the faster fall off being a result of the P $3p$ Cooper minimum. Such a phosphorus contribution to the $7a_1$ and $4e$ orbitals, which are associated with E_3, is generally accepted and is predicted to be *ca.* 15% by SCM-Xα-DV calculations.[27] These calculations, however, predict that the $5e$ level, which gives rise to E_2, is 97% F $2p$. It seems reasonable to us that the $5e$ level is P–F π bonding and that these intensity changes reflect its composite nature.

The r.p.p.i.c.s of all three E bands show some small perturbation between 70 and 90 eV. The b.r. plots in Figure 8(*a*) and (*b*) indicate that E_2 shows a relative increase in intensity over the $p \longrightarrow d$ resonance region (see also Figure 1). As the level to which the p electron is excited in the p–d resonance is delocalized over the PF_3 ligand we might well expect some general appearance of the resonance in these bands.[5] The fact that it is relatively strong in band E_2 suggests a more selective mechanism, and that these electrons have some $3d$ character. Though the $7e$ orbitals of the PF_3 ligand are thought to be the principal ones involved in metal PF_3 back-donation, it is also possible that Ni $3d$ orbitals contribute to the levels derived from the $5e$ orbitals. If these are indeed partially localized on phosphorus as suggested above they are more likely candidates for mixing than the $6e$ PF_3 level which calculations,[27] supported by the cross-section behaviour, suggest to be 99% fluorine localized.

Conclusion

The effects of covalency are seen in the r.p.p.i.c. behaviour of the valence ionizations of $[Ni(PF_3)_4]$ and most features present can be explained on the basis of the Gelius model using atomic cross-section features.

Even though the d shell is formally full being occupied by ten electrons in this zerovalent nickel compound, a $p \longrightarrow d$ resonance is sufficiently strong to be observed in ionizations of m.o.s with Ni $3d$ character. Resonance occurs through excitation of a Ni $3p$ electron to empty $2e$ and $3t_2$ orbitals which are pre-

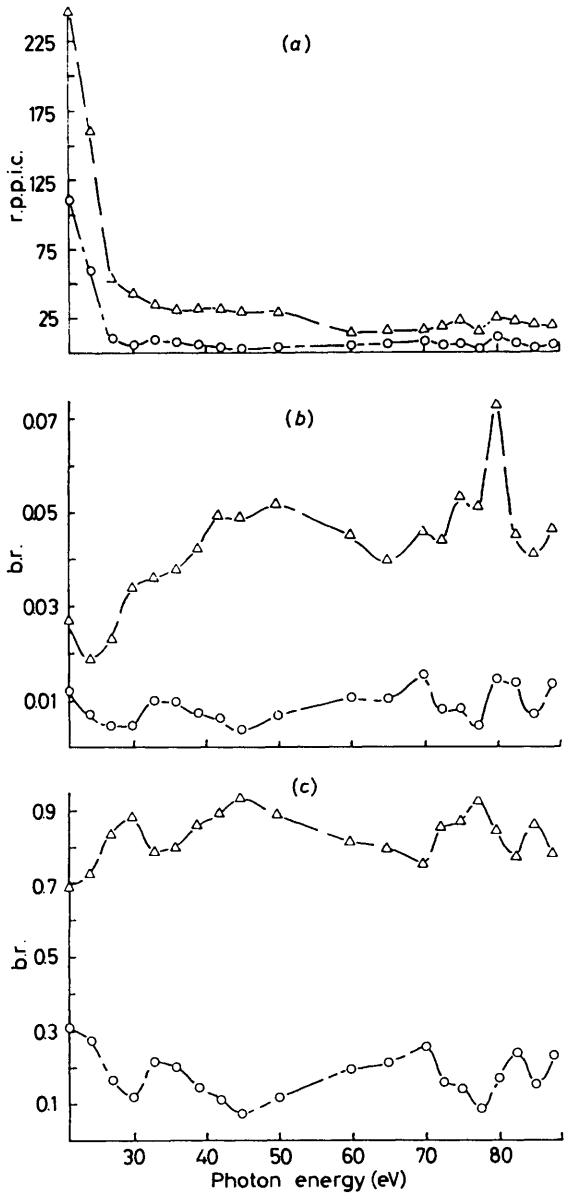

Figure 6. R.p.p.i.c.s and b.r.s for $1t_2$ (△) and a_1 (○) orbitals: (*a*) r.p.p.i.c.s, (*b*) b.r. for $1t_2$ and a_1 relative to whole spectrum, and (*c*) $1t_2/a_1$ b.r.

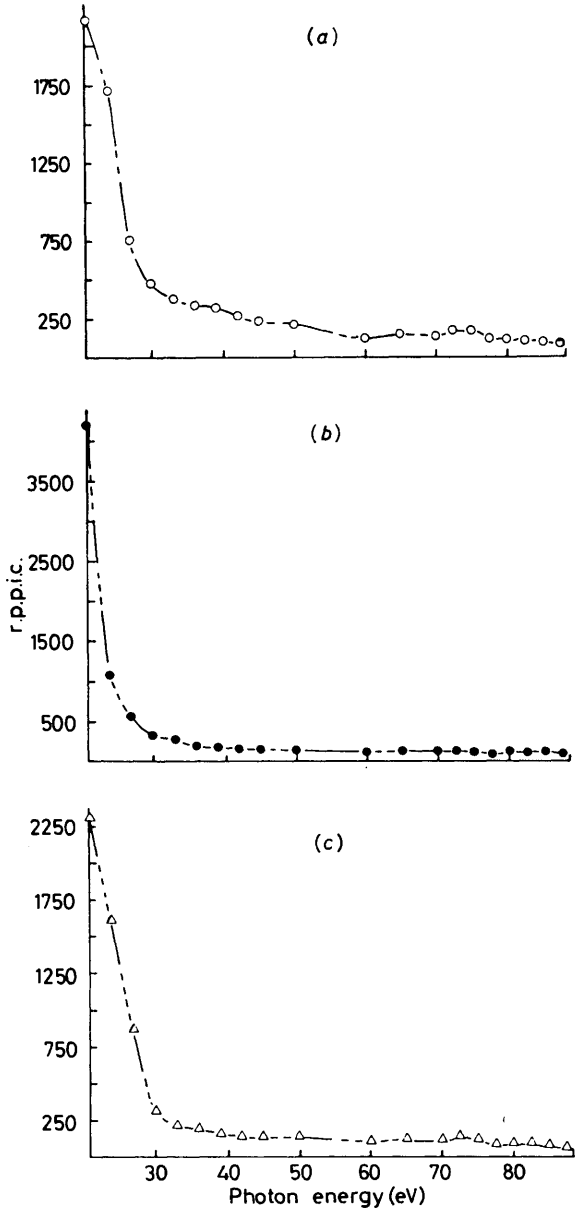

Figure 7. R.p.p.i.c.s for bands in region E: (*a*) E_1, (*b*) E_2, and (*c*) E_3

dominantly P–F based but have some Ni 3*d* character. This might be expected to enable the resonance to be observed in all orbitals and there is some evidence for this in the r.p.p.i.c.s of all valence orbitals, albeit weak for bands E_1 ($6e$, $1a_2$) and E_3($7a$,$4e$). The *p*–*d* resonance is strongest for the $1e$ and $2t_2$ orbitals which are largely nickel based, but also evident in the $1t_2$ orbital which is Ni–P σ bonding.

A molecular shape resonance was seen to enhance the relative intensity of bands from orbitals containing large contributions from Ni 3*d* orbitals at the He II photon energy; this removed the generally observed $2t_2$:$1e$ (3:2) and $1t_2$:a_1 (3:1) statistical intensity ratios expected for the ionizations on the basis of orbital occupancy. The orbitals with a higher Ni 3*d* character gain more in intensity, namely $1e$ more than $2t_2$ and $1t_2$ more than a_1. The $1e$ orbital has no σ interaction with the trifluorophosphine ligands and consequently has a higher Ni 3*d* character. Both the shape resonance and the $p \longrightarrow d$ resonance are stronger for this orbital than for the $2t_2$ orbital.

The P 3*p*-, F 2*p*-, and P–F-based ionizations essentially show a monotonic decrease in r.p.p.i.c. with increasing photon energy. The $1t_2$ orbitals (M–P bonding) which, by symmetry, can mix with the Ni 3*d* orbitals, show small maxima in their r.p.p.i.c.s at the same photon energies as the resonance maxima in the $2t_2$ and $1e$ r.p.p.i.c.s. Small maxima are also seen in the r.p.p.i.c.s of the PF_3-localized ionizations, as the $p \longrightarrow d$ resonance occurs by absorption to the $3t_2$ and $2e$ orbitals which are highly delocalized, and consequently resonant enhancement can be seen in other valence orbitals. The preferential enhancement of the band derived from the PF_3 $5e$ orbitals provides evidence for Ni–P back donation.

The r.p.p.i.c. behaviour of the a_1 orbital is essentially that of P 3*p*, no mixing of this orbital with the Ni 3*d* orbitals is possible, and the expected Cooper minimum is observed.

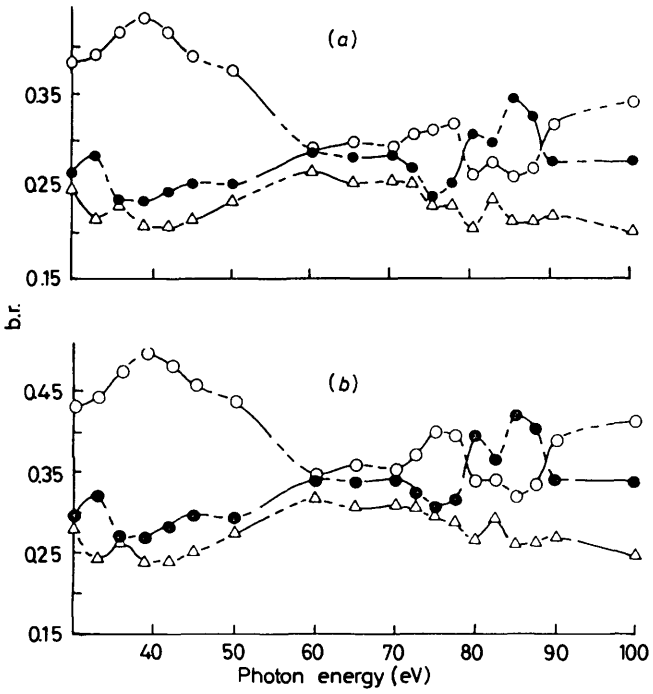

Figure 8. B.r. for bands in region E (○, E_1; ●, E_2; △, E_3): (*a*) relative to whole spectrum and (*b*) $E_1/E_2/E_3$ b.r.

Acknowledgements

We thank the S.E.R.C., the Gateway Corporation, and Lady Margaret Hall for financial support.

References

1 W. C. Price, A. W. Potts, and D. G. Streets, in 'Electron Spectroscopy,' ed. D. A. Shirley, North-Holland, Amsterdam, 1972, p. 187.
2 J. C. Green, *Struct. Bonding (Berlin)*, 1981, **43**, 37.
3 A. W. Potts, I. Novak, F. Quinn, G. V. Marr, B. R. Dobson, and I. I. Hillier, *J. Phys. B*, 1985, **18**, 3177.
4 G. Cooper, J. C. Green, M. P. Payne, B. R. Dobson, and I. H. Hillier, *J. Am. Chem. Soc.*, 1987, **109**, 3836.
5 G. Cooper, J. C. Green, and M. P. Payne, *Mol. Phys.*, 1988, **63**, 1031.
6 J. G. Brennan, J. C. Green, and C. M. Redfern, *J. Am. Chem. Soc.*, 1989, **111**, 2373.
7 J. Barth, F. Gerken, K. L. I. Kobayashi, J. H. Weaver, and B. Sonntag, *J. Phys. C*, 1980, **13**, 1369.
8 J. L. Dehmer, A. F. Starace, U. Fano, J. Sugar, and J. W. Cooper, *Phys. Rev. Lett.*, 1971, **26**, 1521.
9 Th. Kruck, *Angew. Chem., Int. Ed. Engl.*, 1967, **6**, 53.
10 J. F. Nixon, (*a*) *Adv. Inorg. Chem. Radiochem.*, 1970, **13**, 363; (*b*) *Endeavour*, 1973, **32**, 19.
11 J. C. Green, D. I. King, and J. H. D. Eland, *Chem. Commun.*, 1970, 1121.
12 I. H. Hillier, V. R. Saunders, M. J. Ware, P. J. Bassett, D. R. Lloyd, and N. Lynaugh, *Chem. Commun.*, 1970, 1316.
13 P. J. Bassett, B. R. Higginson, D. R. Lloyd, N. Lynaugh, and P. J. Roberts, *J. Chem. Soc., Dalton Trans.*, 1974, 2316.
14 J. B. West and G. V. Marr, *Proc. R. Soc. London, Ser. A*, 1976, **349**, 397.
15 J. B. West and J. Morton, *At. Data Nucl. Data*, 1978, **22**, 103.
16 A. A. Williams, *Inorg. Synth.*, 1957, **5**, 95.
17 (*a*) P. L. Timms, *J. Chem. Soc. A*, 1970, 2526; (*b*) C. M. Redfern, Part II Thesis, Oxford, 1985.
18 R. J. Angelici and C. M. Ingemanson, *Inorg. Chem.*, 1969, **8**, 83.
19 W. A. G. Graham, *Inorg. Chem.*, 1968, **7**, 315.
20 R. Mason and D. W. Meek, *Angew. Chem., Int. Ed. Engl.*, 1978, **17**, 183.
21 B. B. Wayland and M. E. Abn-Elmageed, *J. Am. Chem. Soc.*, 1974, **96**, 4809.
22 R. R. Corederman and J. L. Beauchamp, *Inorg. Chem.*, 1977, **16**, 3135.
23 J. M. Savariault and J. F. Labarre, *Theor. Chim. Acta*, 1976, **42**, 207.
24 J. M. Savariault, A. Serafini, M. Pelissier, and P. Cassoux, *Theor. Chim. Acta*, 1976, **42**, 155.
25 (*a*) J. Chatt, *Nature (London)*, 1950, **165**, 637; (*b*) G. Wilkinson, *J. Am. Chem. Soc.*, 1951, **73**, 5501.
26 I. H. Hillier and V. R. Saunders, *Trans. Faraday Soc.*, 1970, **66**, 2401.
27 S-X. Xiao, W. C. Trogler, D. E. Elliss, and Z. Berkovitch Yellin, *J. Am. Chem. Soc.*, 1983, **105**, 7033.
28 D. Marynick, *J. Am. Chem. Soc.*, 1984, **106**, 4064.
29 A. G. Orpen and N. G. Connelly, *J. Chem. Soc., Chem. Commun.*, 1985, 1310.
30 J. P. Maier and D. W. Turner, *J. Chem. Soc., Faraday Trans. 2*, 1972, 711.
31 M. B. Robin, *Chem. Phys. Lett.*, 1985, **119**, 33.
32 D. Briggs (ed.), 'Handbook of *X*-Ray and Ultraviolet Photoelectron Spectroscopy,' Heyden, London, 1977.
33 J. J. Yeh and I. Lindau, *At. Data Nucl. Data Tables*, 1985, **32**, 1.
34 T. A. Carlson, A. Fahlman, M. O. Krause, T. Whitley, and F. A. Grimm, *J. Chem. Phys.*, 1984, **81**, 5389.
35 I. Novak, J. M. Benson, and A. W. Potts, *Chem. Phys.*, 1986, **104**, 153.
36 B. W. Yates, K. H. Tan, G. M. Bancroft, L. L. Coatsworth, and J. S. Tse, *J. Chem. Phys.*, 1985, **83**, 4906.
37 T. A. Carlson, C. A. Fahlman, W. A. Svensson, M. O. Krause, T. A. Whitley, F. A. Grimm, M. N. Piancastelli, and J. W. Taylor, *J. Chem. Phys.*, 1984, **81**, 3828.
38 H. Daamen, G. Boxhoorn, and A. Oskam, *Inorg. Chim. Acta*, 1978, **28**, 263.

Received 7th September 1989; *Paper* 9/03825F